Effects of P on amorphous chemical vapor deposition Ru-P alloy films for Cu interconnect liner applications

Jinhong Shin
Materials Science and Engineering, University of Texas at Austin, Austin, Texas 78712

Hyun-Woo Kim
Chemical Engineering, University of Texas at Austin, Austin, Texas 78712

Kyriacos Agapiou and Richard A. Jones
Chemistry and Biochemistry, University of Texas at Austin, Austin, Texas 78712

Gyeong S. Hwang and John G. Ekerdt[a)]
Chemical Engineering, University of Texas at Austin, Austin, Texas 78712

(Received 1 October 2007; accepted 3 December 2007; published 1 July 2008)

Amorphous Ru(P) films grown by chemical vapor deposition at 575 K using a single source precursor, *cis*-$RuH_2(P(CH_3)_3)_4$, or dual sources, $Ru_3(CO)_{12}$ and $P(CH_3)_3$ or $P(C_6H_5)_3$, are studied. The phosphorus percentage affects the film microstructure, and incorporating >13% P resulted in amorphous Ru(P) films. While codosing $P(CH_3)_3$ with $Ru_3(CO)_{12}$ improves film step coverage, the most conformal Ru(P) film is obtained with *cis*-$RuH_2(P(CH_3)_3)_4$. A fully continuous 5 nm Ru(P) film is formed within 1 μm deep, 8:1 aspect ratio trenches. The barrier performance is tested using Cu/Ru/Si(100) stacks annealed at 575 K, and sheet resistance was used as a measure of barrier failure. Cu diffusivity in physical vapor deposition (PVD) Ru is approximated to be 6.6×10^{-17} cm^2/s at 575 K, which indicates fast Cu diffusion along the grain boundaries. While 26 nm polycrystalline PVD Ru failed after 6 h annealing by Cu penetration, 28 nm amorphous Ru(P) survived after 67 h annealing. First principles density functional calculations suggest 16.7% P degraded the adhesion strength by 12% when compared to crystalline Cu/Ru, by the presence of P at the interface. However, due to the strong Ru-Cu bonds, amorphous Ru(P) still forms a stronger interface with Cu than do Ta and TaN to Cu, as observed when annealing 10 nm Cu films on these surfaces at 675 K. © *2008 American Vacuum Society.* [DOI: 10.1116/1.2832360]

I. INTRODUCTION

Copper has replaced aluminum as the interconnect material in advanced very large-scale integration (VLSI) devices due to its superior electrical conductivity and intrinsic electromigration (EM) resistance, which brought about significant changes in processes and materials. Liner materials are placed between Cu and an intermetal dielectric to prevent Cu diffusion and improve adhesion. The liner can include an adhesion promoting layer, a diffusion barrier, and a Cu seed layer, and currently, a physical vapor deposition (PVD) TaN/Ta/Cu stack is most widely used. However, due to the poor step coverage of PVD, and the thickness requirements for sub 32 nm devices,[1] extensive studies have been performed in the search for new liner materials.[2,3]

Ru has been considered as a promising liner material for its low resistivity, chemical inertness, strong adhesion with Cu, and low Cu solubility. However, the 3D mode (Volmer-Weber) growth of Ru makes it difficult to form conformal and thin films of a few nanometers, especially inside of high aspect ratio damascene features. The microstructure of Ru films, which is polycrystalline with columnar grains, leads to a poor Cu diffusion barrier performance.[4,5] Alloying Ru to generate an amorphous film is one approach to form conformal thin films that may function as the seed layer and diffusion barrier.

We have recently reported chemical vapor deposition (CVD) amorphous Ru(P) alloy films containing ~15% P (note, compositions on an atom basis) grown at 575 K using a single chemical source, $RuH_2(PMe_3)_4$ (Me=CH_3), which remain amorphous upon annealing at 675 K for 3 h.[6] First principles density functional theory (DFT) calculations indicated $p-d$ hybridization between P and Ru atoms, which contributed to stabilizing the Ru(P) alloy structure. Amorphous Ru(P) alloys were energetically favored over crystalline Ru(P) when the percentage of P was greater than 20%. Surface studies illustrated that the P incorporated by a stepwise demethylation of adsorbed $P(CH_3)_3$,[7] and this suggested the possibility of forming amorphous Ru(P) alloy films using dual chemical sources. Indeed, amorphous Ru(P) films could be formed using $Ru_3(CO)_{12}$ and $P(CH_3)_3$ or $P(C_6H_5)_3$, and a 15 nm amorphous Ru(P) film containing ~15% P was formed at 575 K.[8] Using low-energy ion scattering spectroscopy (LEISS) and x-ray photoelectron spectroscopy (XPS), the thinnest continuous Ru(P) film grown from $Ru_3(CO)_{12}$ and $P(CH_3)_3$ on SiO_2 was 7.1 nm, and ~0.4 nm Cu (i.e., 2–3 monolayers) wetted on the Ru(P) surface having ~15% P.

a)Electronic mail: ekerdt@che.utexas.edu

In this study, we report how film properties, required for barrier/seed application, are affected by the presence of P in Ru(P) films grown with $RuH_2(PMe_3)_4$, or $Ru_3(CO)_{12}$ and $P(CH_3)_3$. The effect of P and C concentrations on microstructure and film resistivity is explored using XPS, x-ray diffraction (XRD), and a four-point probe. The step coverage of Ru and Ru(P) films is analyzed with cross-sectional transmission electron microscopy (TEM). The barrier property and Cu adhesion of amorphous Ru(P) films are evaluated by annealing studies, and first principles DFT calculations are performed to understand the impact of P at the Cu/Ru(P) interface.

II. EXPERIMENT

Film growth was carried out in a deposition and analysis facility consisting of a vacuum sample transfer system, load lock, XPS system (Physical Electronics 3057; Mg $K\alpha$), CVD chamber, and a PVD chamber equipped with direct current magnetron sputtering guns. The stainless-steel CVD chamber is a cold-wall vessel (base pressure 6.7×10^{-6} Pa) and the SiO_2/Si(100) substrates were heated radiatively from below. Thermally grown SiO_2/Si(100) 200 mm wafers were supplied by Sematech. The wafers were cut into 20×20 mm pieces and heated to the growth temperature under vacuum. For barrier tests, SiO_2 was removed before Ru(P) deposition using TIMETCH^{TM} solution for 10 min. The synthesis of $RuH_2(PMe_3)_4$ is described elsewhere;[9] the solid compound was sublimed at 355 K to obtain sufficient vapor pressure and delivered to the CVD chamber using flowing Ar through a heated gas line and shower head. $Ru_3(CO)_{12}$ (Strem Chemical; 99%) was sublimed at 355 K and delivered to the CVD chamber using 2.5–5.0 standard cm^3 per min (sccm) of flowing H_2 through a heated gas line and shower head. $P(C_6H_5)_3$ (Strem Chemical, 99%) was sublimed at 335 K and delivered using 5–10 sccm of flowing Ar through separately heated lines. $P(CH_3)_3$ (Strem Chemical, 99%) was dosed directly into the reaction chamber; the flow was controlled using a leak valve. The deposition was carried out at 30–50 Pa. *Ex situ* XPS chemical state analysis was performed with a Physical Electronics 5700, which is fitted with a monochromatic Al $K\alpha$ source. Crystallinity is established using grazing angle (1°) XRD (Bruker-Nonius D8). TEM analysis was performed with a JOEL 2010F or FEI TECNAI G2 F20 operated at 200 kV. LEISS was carried out *in situ* using 1 kV He^+. The samples were sputter cleaned with 2 kV Ar^+ before both XPS and LEISS.

Atomic structure and energy calculations were performed using the DFT program package VASP (Vienna *ab initio* Simulation Package) with the generalized gradient approximation (GGA) function derived by Perdew and Wang (PW91). A plane-wave basis set for valence electron states and Vanderbilt ultrasoft pseudopotentials for core-electron interactions were employed, and Brillouin zone sampling was performed using Monkhorst-Pack-type k-point meshes. A plane-wave cutoff energy of 400 eV was used, and the Brillouin zone integration was performed using a $2\times2\times1$ k-point mesh. All atoms were fully relaxed using the conjugated gradient method until residual forces on constituent atoms became smaller than 5×10^{-2} eV/Å.

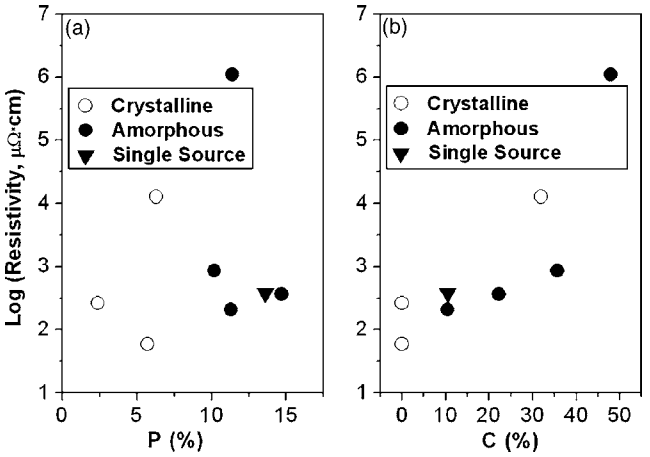

FIG. 1. Electrical resistivity of amorphous and crystalline Ru(P) films grown with $Ru_3(CO)_{12}$ and $P(CH_3)_3$ or $P(C_6H_5)_3$ at 575 K as a function of (a) P percentage, and (b) C percentage in the films.

III. RESULTS AND DISCUSSION

Figure 1 presents the influence of P and C concentrations on the microstructure and the electrical resistivity of Ru(P) films grown from $Ru_3(CO)_{12}$ and $P(CH_3)_3$ or $P(C_6H_5)_3$ at 575 K. The P and C concentrations are determined by XPS. Due to the overlapping C 1s and Ru 3d XPS peaks, and vastly different sensitivity factors, calculating the C concentration in Ru is not straightforward; however this can be overcome by fitting the Ru $3d_{5/2}$ and $3d_{3/2}$ peaks, assuming pure Ru has a peak intensity ratio of 1.5 based on the relative degeneracy of the 3d doublet peaks. Measurement and fitting conditions are carefully optimized using a 99.95% PVD Ru target to minimize possible fitting errors.

The microstructure of Ru(P) alloy films is closely related to the P concentration in the films, as shown in Fig. 1(a). The films containing more than ~13% P, on a C-free basis, feature an amorphous microstructure. Our previous *ab initio* molecular dynamics calculation demonstrated that the amorphous phase was most stable when more than 20% of P was incorporated, and experimentally the minimum P concentration in the amorphous Ru(P) in this study is ~13%, on a C-free basis. The difference between the experiment (13% P) and the simulation (20% P) could be attributed to the effect of the C impurity, which was not considered in the calculations, or possible microscopic nonuniform P distribution in the Ru(P) films.[10]

Carbon does not have a significant impact on microstructure, as shown in Fig. 1(b). Possibly because of the small atomic size of C, it preferentially locates in interstitial sites in the disordered lattice of Ru(P) rather than substituting for Ru or P sites. Although further study will be needed to understand how C exists in Ru(P) alloys, the lack of Ru-C compounds and strong Ru-Ru and C-C bonds suggests that C would not be an efficient alloying element for a stable amorphous Ru alloy. Unlike Ru-C, the Ru-P system features pos-

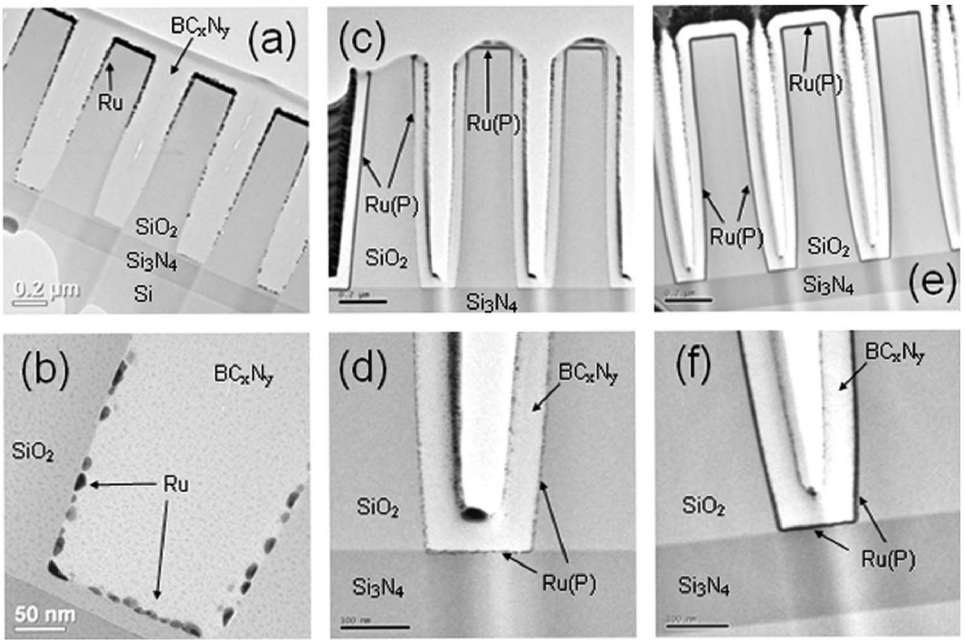

FIG. 2. Cross-sectional TEM images of (a) and (b) the CVD Ru film grown with $Ru_3(CO)_{12}$ only at 475 K; (c) and (d) the CVD Ru(P) film grown with the dual source, $Ru_3(CO)_{12}$ and $P(CH_3)_3$, at 575 K; and (e) and (f) the CVD Ru(P) film grown with the single source precursor, $RuH_2(PMe_3)_4$, at 575 K.

sible Ru_2P, RuP, and RuP_2 compounds, and this chemical interaction between Ru and P may also be a contributing factor in amorphous alloy formation during CVD.[11] Interactions between Ru and P are also supported by our previous density of state (DOS) analysis of amorphous Ru(P) alloys, which indicates hybridization between Ru 4*d* and P 3*p* orbitals.[8] Carbon impurities strongly and negatively impact the electrical resistivity as shown in Fig. 1(b); the resistivity increases with higher C content in Ru(P) films. According to the DOS analysis, amorphous Ru(P) alloy containing 20% P is metallic, and impurities like C can act as scattering centers for electron transfer, degrading the electrical conductance of Ru(P) films. The lowest resistivity for an amorphous Ru(P) alloy containing 11.3% P and 10.5% C was 210 $\mu\Omega$ cm.

Figure 2 presents the step coverage in trench patterns of the crystalline Ru film grown with $Ru_3(CO)_{12}$ only and the amorphous Ru(P) films from $RuH_2(PMe_3)_4$ and $Ru_3(CO)_{12}$ with $P(CH_3)_3$. The trenches are ~ 1.0 μm deep and 0.13 -0.18 μm wide. The substrate temperatures during film growth are 475 and 575 K for Ru and Ru(P) films, respectively. The lower substrate temperature for Ru from $Ru_3(CO)_{12}$ likely enhances the step coverage by suppressing the reactive sticking coefficient of $Ru_3(CO)_{12}$. Precursor molecules that strike a surface undergo either decomposition (reaction), desorption, or diffusion, and higher substrate temperatures degrade the step coverage because the decomposition rate increases much more rapidly than desorption and diffusion rates as temperature increases.[12] However, even with the lower temperature and larger trenches, most of the CVD Ru is found near the top of trenches, and only some grains are visible within the trenches. The large size ($\sim$15 nm) and low density of grains indicates a strong 3D (Volmer-Weber) growth mode of Ru due to its high surface energy ($\gamma_{Ru(001)}=3.05$ J/m^2 and $\gamma_{SiO_2}=1.15-2.00$ J/m^2).[13,14]

Amorphous Ru(P) from $Ru_3(CO)_{12}$ and $P(CH_3)_3$ shows improved coverage compared to Ru, although it is not fully continuous in the trenches. This can be explained by the reduced adsorption/reaction sites available for $Ru_3(CO)_{12}$ in the presence of $P(CH_3)_3$. $P(CH_3)_3$ adsorbs on the Ru surface as low as 80 K and undergoes complete demethylation to P by 450 K.[7] Possibly due to the adsorbed $P(CH_3)_3$, $Ru_3(CO)_{12}$ has less chance of finding an adsorption/reaction site, and will have a greater possibility to migrate deeper into the trenches. The reduced reactivity of $Ru_3(CO)_{12}$ with $P(CH_3)_3$ is also supported by the lower growth rate with higher $P(CH_3)_3$ dosing. The growth rates of Ru(P) with 5.7% and 11.3% P are 5.7 and 2.5 Å/min, respectively.

At the bottom of the trench, Ru(P) from the dual sources also features a 3D growth mode as shown in Fig. 2(d); however, the grains are much smaller and more crowded than for Ru [Fig. 2(b)], which can be explained by the differences in nucleation densities of amorphous and crystalline phases. According to the capillary theory of heterogeneous nucleation, nucleation energy and the ratio of nucleation rates of amorphous and crystalline phases can be expressed as[15]

$$G^* = \frac{16\pi}{3}\frac{\gamma^3\nu^2}{\Delta G^2}f(\theta), \tag{1}$$

$$\frac{N_a}{N_c} = \exp\left[\frac{(G_c^* - G_a^*)}{kT}\right], \tag{2}$$

where γ is the surface energy, ν is the molar volume, ΔG is the Gibbs energy for the reaction, $f(\theta)$ is the shape factor, which is a function of the contact angle, θ, and N is the nucleation density. The subscripts a and c denote the amorphous and crystalline phases, respectively. Comparing the nucleation energies for amorphous Ru(P) and crystalline Ru is not straightforward because of the different film composi-

tion and growing conditions. However, simple arguments can be made by assuming that the molar volumes and shape factors are equal for both films. These are reasonable assumptions considering that the molar volume of amorphous and crystalline metal alloys differs by only a few percent,[8] and both Ru(P) and Ru have a 3D growth mode on SiO_2. Therefore, provided that ΔG of both films are similar, the nucleation energy, G^*, strongly depends on the surface energies. The surface energy, and thus the nucleation energy, of amorphous Ru(P) should be lower than those of crystalline Ru because of its random structure and the dilution effect by a low surface energy element, P. Faster nucleation of metastable phases than of stable phases is found in many systems, such as condensation of supercooled liquid or saturated gas phases,[16] and solid-state reactions.[17] This phenomenon is known as Ostwald's step rule, which is explained with the lower nucleation energy and smaller critical nuclei size of metastable phases.[18,19] A higher nucleation density is beneficial in forming thinner films, especially when growth follows a 3D mode. Indeed, our previous study shows that ~7 nm Ru(P) grown with the dual sources on SiO_2 is fully continuous based on LEISS analysis,[8] while crystalline CVD Ru from $Ru_3(CO)_{12}$ needs ~20 nm of film to become continuous on SiO_2.[20] The film thickness is established using the attenuation of the XPS Si 2*p* peak, and confirmed with TEM analysis.

The best step coverage is obtained with the Ru(P) films grown with $RuH_2(PMe_3)_4$, as shown in Figs. 2(e) and 2(f). The Ru(P) film is fully continuous within the trenches of an 8:1 aspect ratio, and the film thicknesses at the top and in the trench are 8 and 5 nm, respectively. Considering that both single and dual sources have $P(CH_3)_3$ that reduces the available adsorption/reaction sites for Ru precursors, the different Ru(P) film step coverage can be explained by differences in the reactive sticking coefficient of the Ru precursors. $Ru_3(CO)_{12}$ can easily lose carbonyl ligands to leave Ru behind; however, complete decomposition may be more difficult for $RuH_2(PMe_3)_4$. This is supported by the fact that Ru(P) film can be grown with $RuH_2(PMe_3)_4$ above 525 K, while Ru films are grown with $Ru_3(CO)_{12}$ at temperatures as low as 425 K.[21] The lower reactivity of $RuH_2(PMe_3)_4$ offers it more chance to migrate into the trenches and form more conformal films.

The potential barrier property of CVD Ru(P) film grown with the dual source is compared with PVD Ru films by measuring the sheet resistances with a four-point probe after annealing. The films are placed between a Si(100) substrate and 150 nm PVD Cu, and annealed at 575 K under N_2/H_2 gas for various times. Since Ru-silicide, which degrades film integrity, can be formed at ~675 K, a relatively low annealing temperature is used in this study. Several studies show that PVD Ru films have a poor barrier property.[4,5] Coincidently, our study shows that a 6.5 nm PVD Ru film impeded Cu diffusion for 15 min, but failed after 60 min based on the resistance as shown in Fig. 3. An initial decrease in resistance is due to grain growth and defect removal in Cu. As Cu diffuses through the Ru film to form Cu-silicide, a significantly increased resistance is recorded as shown in Fig. 3. A thicker PVD Ru requires a longer annealing time for failure, and 26 nm PVD Ru fails after 360 min annealing. Although the exact failure time is not clear on the annealing study, Cu diffusivity can be roughly estimated. The average diffusion length of Cu can be determined by[22]

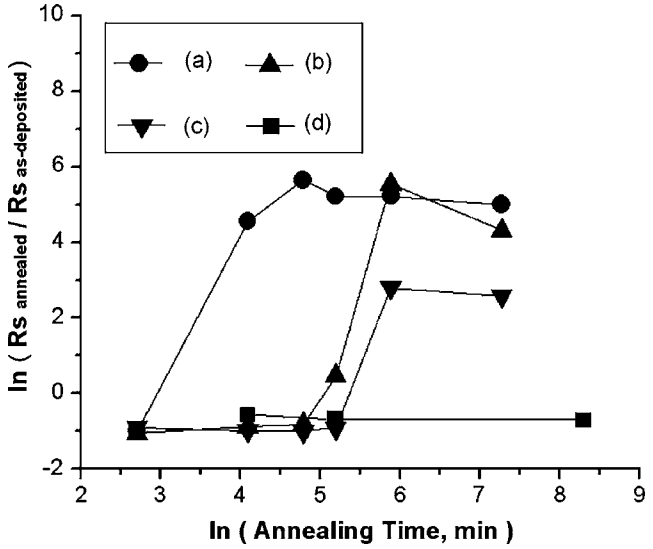

FIG. 3. Changes in the sheet resistance of 150 nm PVD Cu / PVD Ru or CVD Ru(P) / Si stacks before and after annealing at 575 K for various annealing times. (a) 6.5 nm PVD Ru; (b) 13 nm PVD Ru; (c) 26 nm PVD Ru; and (d) 28 nm amorphous CVD Ru(P) grown with $Ru_3(CO)_{12}$ and $P(CH_3)_3$ at 575 K.

$$L^2 = 4Dt, \tag{3}$$

where L is diffusion length, D is Cu diffusivity, and t is annealing time. The diffusivity of Cu in PVD Ru is determined to be 6.6×10^{-17} cm^2/s at 575 K. Cu diffusivity data in Ru are not reported. Herein, we compare it with Cu diffusivity in TaN films (Table I) to illustrate a possible diffu-

TABLE I. Cu diffusivity in TaN films.

	Barrier	Diffusion path	$D_0(cm^2/s)$	E_a(eV)	D_{Cu} at 575 K(cm^2/s)	Ref.
(a)	PVD TaN	Lattice	160	3.27	3.6×10^{-27}	28
(b)	PVD TaN	Lattice	6.7×10^{-4}	2.7	1.9×10^{-27}	29
(c)	PVD TaN	Grain boundary	2.36×10^{-11}	0.8	2.3×10^{-18}	30
(d)	PVD TaN	Grain boundary	2.8×10^{-10}	1.3	1.1×10^{-21}	29
(e)	ALD TaN	Grain boundary	6.2×10^{-9}	1.2	2.0×10^{-19}	31

sion path. Cu diffusivities are calculated using the reported D_0 and E_a values. The Cu diffusivity in PVD Ru is significantly higher than the diffusivity in a TaN lattice, and comparable to the Cu diffusivities through TaN grain boundaries. This suggests that Cu is penetrating the PVD Ru along the grain boundaries. TaN films (d) and (e) in Table I are reported to be polycrystalline, having disordered grain boundaries, and TaN film (c) has a columnar structure with larger and ordered grain boundaries. The grain boundary diffusion is dependent on the microstructure of the barrier films, and the columnar structure is known to have the poorest barrier performance.[3] Cu diffusivity in Ru is even higher than the diffusivity in TaN film (c), confirming that PVD Ru is not an appropriate barrier for Cu diffusion. On the other hand, CVD Ru(P) film, having a comparable thickness with the PVD Ru that failed after 360 min annealing, does not show an increase in resistance after 4020 min (67 h) annealing. Although Cu diffusivity in CVD Ru(P) film could not be determined because it did not fail, the result suggests a superior barrier property of amorphous Ru(P) over PVD Ru having a columnar structure. The advantage of amorphous films in blocking Cu diffusion can be found elsewhere,[23,24] and amorphous Ru(P) is expected to have an improved barrier capability over polycrystalline Ru. However, to be noted here is that the Ru(P) film grown with the dual source on Si(100) does not feature a fully amorphous microstructure, possibly due to the film growth on a single crystalline substrate. While the barrier performance of a 26-nm-thick Ru(P) film is encouraging, barrier performance needs to be established for 2–3-nm-thick Ru(P) using bias thermal stress or triangular voltage sweep techniques to determine if Ru(P) could function as a barrier for 32 nm interconnects.

Cu adhesion with CVD Ru(P), PVD Ta, and PVD TaN films was studied using LEISS and XPS after annealing at 675 K for 1 h with N_2/H_2. Amorphous Ru(P) film containing ~15% P was grown on SiO_2 with $Ru_3(CO)_{12}$ and $P(CH_3)_3$, and the 10 nm PVD Cu was deposited on 30 nm Ru(P), Ta, and TaN without exposure to air. LEISS is very surface sensitive due to the low kinetic energy of He^+ ions. Figure 4(A) shows that the surface is fully covered with Cu atoms before annealing. Ta peaks emerge at $E/E_0=0.89$ for the Cu/Ta and Cu/TaN samples after annealing; however, only the Cu peak is visible at $E/E_0=0.80$ for the Cu/Ru(P) sample, indicating a stronger Cu adhesion with Ru(P) than Ta or TaN. Assuming the Cu/Ru(P) surface is completely covered with Cu, and ignoring any attenuation effect of photoelectrons, the Cu surface coverage can be determined from the intensity ratio of the XPS Cu $2p_{3/2}$ peaks at 932.6 eV referenced against Cu/Ru(P). From Fig. 4(B), the Cu coverages on Ta and TaN after annealing are 63% and 26%, respectively. This is consistent with the studies that show a stronger Cu adhesion with Ta than TaN; from contact angle measurements, the adhesion energies of Cu/Ta and Cu/TaN were reported to be, respectively, 2.17 and 1.85 J/m^2,[25] and first principles DFT calculation also showed ~20% lower adhesion strength in Cu/TaN than Cu/Ta.[26]

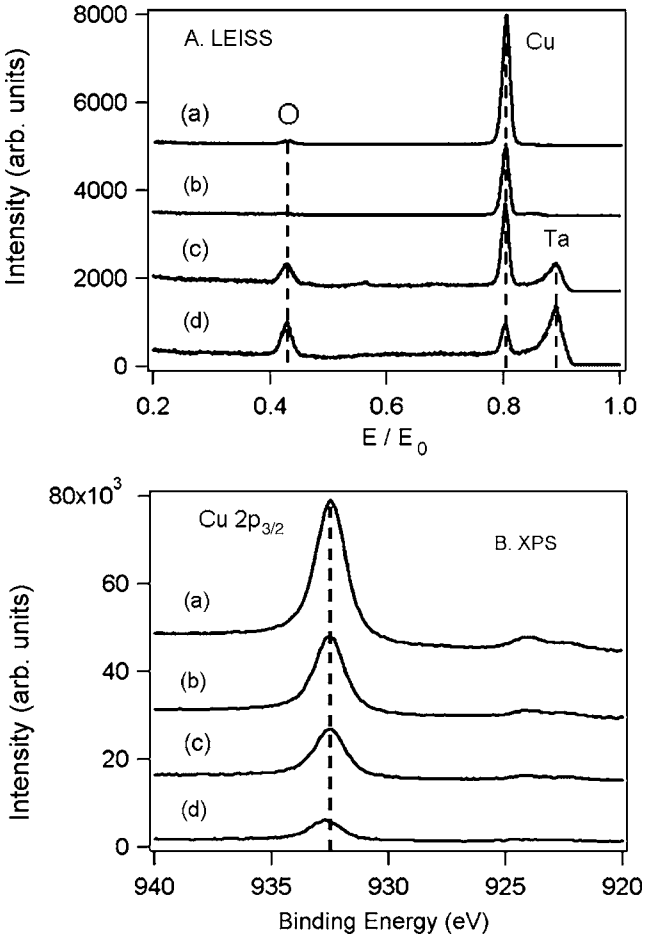

FIG. 4. LEISS result (A) and XPS Cu $2p_{3/2}$ peak (B) of (a) PVD Cu without annealing; (b) after annealing PVD Cu/30 nm CVD Ru(P) grown with $Ru_3(CO)_{12}$ and $P(CH_3)_3$; (c) PVD Cu / 30 nm PVD Ta; and (d) PVD Cu / 30 nm PVD TaN.

In order to understand the impact of P on Cu adhesion in amorphous Ru(P) films, the ideal work of separation, which is the work required to separate a unit area of interface, was calculated using the first principles DFT. The ideal work of separation, W_{sp}, can be defined as follows:

$$W_{sp}=\frac{(E_{\mathrm{Cu}}+E_{\mathrm{Ru}}-E_{\mathrm{Cu/Ru}})}{A}, \tag{4}$$

where $E_{\mathrm{Cu/Ru}}$ is the total energy of a Cu/Ru supercell, E_{Cu} and E_{Ru} are the total energies of Ru and Cu slabs with vacuum, respectively, and A is the total interface area. The supercells explored in this study, c-Cu/c-Ru a-Cu/a-Ru, and a-Cu/a-Ru(P) with 16.7% P, are shown in Fig. 5. The 16.7% P is at the Cu/Ru interface, and the subscripts a and c denote amorphous and crystalline phases, respectively. The c-Cu/c-Ru and a-Cu/a-Ru supercells are composed of 60 Cu/60 Ru and 60 Cu/72 Ru atoms, respectively, and two Ru atoms at the a-Cu/a-Ru interface are substituted with P atoms to generate the a-Cu/a-Ru(P) supercell. Normalized W_{sp} of a-Cu/a-Ru and a-Cu/a-Ru, based on c-Cu/c-Ru, are 1.06 and 0.88, respectively. Considering that amorphizing Cu and Ru interface enhances the adhesion strength (W_{sp}) by

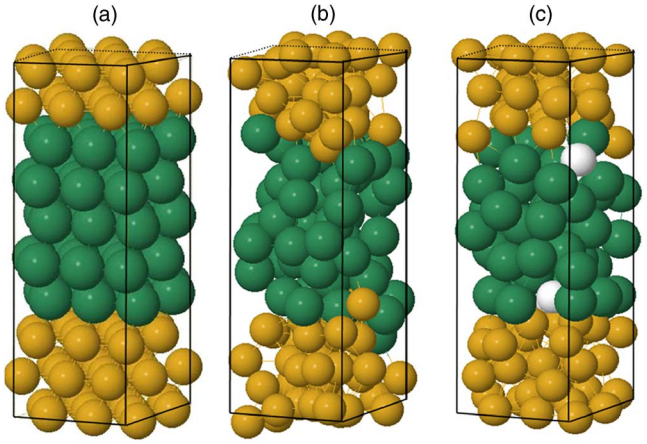

FIG. 5. Cu/Ru interface model structures used in the DFT calculation for W_{sp}. (a) c-Cu/c-Ru; (b) a-Cu/a-Ru; and (c) a-Cu/a-Ru(P) with 16.7% P. Large gray and dark balls represent Cu and Ru atoms, respectively, and small white balls indicate P atoms.

6%, placing 16.7% P at the Cu/Ru interface degraded adhesion strength by 17%, suggesting that P terminates strong Cu-Ru bonds at the interface. From the c-Cu/c-Ru contact angle value reported,[27] the adhesion energy is determined to be 2.94 J/m^2 assuming the surface energy of Cu is 1.7 J/m^2. Considering the 12% decrease in W_{sp} between c-Cu/c-Ru and a-Cu/a-Ru(P) with 16.7% P at the interface, the adhesion energy of a-Cu/a-Ru(P) is approximated to be 2.59 J/m^2. Although P degrades adhesion with Cu, the adhesion energy is still higher than those of Cu/Ta (2.17 J/m^2) and Cu/TaN (1.85 J/m^2),[25] because of the strong Cu-Ru bonds.

IV. SUMMARY

Amorphous Ru(P) films are chemically grown at 575 K using a single source, $RuH_2(PMe_3)_4$, or dual sources, $Ru_3(CO)_{12}$ and $P(CH_3)_3$ or $P(C_6H_5)_3$. P concentration shows a dominant impact on the film microstructure; however, C impurity which is not an efficient amorphizing element, degrades the electrical conductivity. While improved step coverage is obtained in the presence of $P(CH_3)_3$ with $Ru_3(CO)_{12}$, the most conformal Ru(P) film is formed with $RuH_2(PMe_3)_4$. Cu diffusivity in PVD Ru is approximated to be 6.6×10^{-17} cm^2/s at 575 K, suggesting Cu diffusion along PVD Ru grain boundaries. The superior barrier property of amorphous Ru(P) relative to PVD Ru is observed in the annealing study at 575 K. First principles DFT calculations suggest 12% degraded adhesion strength for the amorphous a-Cu/a-Ru(P) with 16.7% P at the interface compared to the crystalline Cu/Ru interface. However, due to the strong Ru-Cu bonds, amorphous Ru(P) still forms stronger adhesion to Cu than do Ta and TaN to Cu, as observed in the annealing study performed at 675 K.

ACKNOWLEDGMENTS

This work was supported by the Semiconductor Research Corporation (Contract 2005-KC-1292.016), the National Science Foundation (Grant CTS-0553839), and the Robert A. Welch Foundation (Grant F-816).

[1]International Technology Roadmap for Semiconductors, 2006 Update, http://public.itrs.net (2006).
[2]H. Kim, J. Vac. Sci. Technol. B **21**, 2231 (2003).
[3]A. E. Kaloyeros and E. Eisenbraun, Annu. Rev. Mater. Sci. **30**, 363 (2000).
[4]R. Chan, T. N. Arunagiri, Y. Zhang, O. Chyan, R. M. Wallace, M. J. Kim, and T. Q. Hurd, Electrochem. Solid-State Lett. **7**, G154 (2004).
[5]J. Tan, X. Qu, Q. Xie, Y. Zhou, and G. Ru, Thin Solid Films **504**, 231 (2006).
[6]J. Shin, A. Waheed, W. A. Winkenwerder, H.-W. Kim, R. A. Jones, G. S. Hwang, and J. G. Ekerdt, Thin Solid Films **515**, 5298 (2007).
[7]H.-S. Tao, U. Diebold, N. D. Shinn, and T. E. Madey, Surf. Sci. **375**, 257 (1997).
[8]J. Shin, H.-W. Kim, G. S. Hwang, and J. G. Ekerdt, Surf. Coat. Technol. **201**, 9256 (2007).
[9]J. Shin, A. Waheed, K. Agapiou, W. A. Winkenwerder, H.-W. Kim, R. A. Jones, G. S. Whang, and J. G. Ekerdt, J. Am. Chem. Soc. **128**, 16510 (2006).
[10]T. Egami and Y. Waseda, J. Non-Cryst. Solids **64**, 113 (1984).
[11]V. B. Chernogorenko, V. G. Ivanchenko, and L. Ya. Kulik, in *Binary Phase Diagrams*, edited by T. B. Massalski, H. Okamoto, P. R. Subramanian, and L. Kacprzak (ASM International, Materials Park, OH, 1990), p. 2979.
[12]G. B. Raupp and T. S. Cale, Chem. Mater. **1**, 207 (1989).
[13]H. L. Skriver and N. M. Rosengaard, Phys. Rev. B **46**, 7157 (1992).
[14]P. Staszczuk, B. Janczuk, and E. Chibowski, Mater. Chem. Phys. **12**, 469 (1985).
[15]H. Ohring, *Materials Science of Thin Films*, 2nd ed. (Academic, San Diego, CA, 2002).
[16]M. Birkholz, B. Selle, W. Fuhs, S. Christiansen, H. P. Strunk, and R. Reich, Phys. Rev. B **64**, 085402 (2001).
[17]K. N. Tu, S. R. Herd, and U. Gösele, Phys. Rev. B **43**, 1198 (1991).
[18]W. Ostwald, Z. Phys. Chem. **22**, 306 (1897).
[19]I. N. Stranski and D. Totomanow, Z. Phys. Chem. **A168**, 399 (1933).
[20]J. Shin, D. Gay, Y.-M. Sun, J. M. White, and J. G. Ekerdt, AIP Conf. Proc. **788**, 482 (2005).
[21]Q. Wang, J. G. Ekerdt, D. Gay, Y. Sun, and J. M. White, Appl. Phys. Lett. **84**, 1380 (2004).
[22]P. Shewmon, *Diffusion in Solids*, 2nd ed. (The Minerals, Metals, and Materials Society, Warrendale, PA, 1989).
[23]H. Kim, C. Cabral, Jr., C. Lavoie, and S. M. Rossnagel, J. Vac. Sci. Technol. B **20**, 1321 (2002).
[24]R. Hübner, M. Hecker, N. Mattern, A. Voss, J. Acker, V. Hoffmann, K. Wetzig, H.-J. Engelmann, E. Zschech, H. Heucer, and Ch. Wenzel, Thin Solid Films **468**, 183 (2004).
[25]O. van der Straten, Y. Zhu, J. Rullan, K. Dunn, and K. E. Kaloyeros, J. Mater. Res. **21**, 255 (2006).
[26]H. Simka, S. Shankar, C. Duran, and M. Haverty, Mater. Res. Symp. Proc. **863**, B9.2.1 (2005).
[27]H. Kim, Y. Naito, T. Koseki, T. Ohba, T. Ohta, Y. Kojima, H. Sato, and Y. Shimogaki, Jpn. J. Appl. Phys. **45**, 2497 (2006).
[28]H. Wang, A. Tiwari, X. Zhang, A. Kvit, and J. Narayan, Appl. Phys. Lett. **81**, 1453 (2002).
[29]T. Oku, E. Kawakami, M. Uekubo, K. Takahiro, S. Yamaguchi, and M. Murakami, Appl. Surf. Sci. **99**, 265 (1996).
[30]J. Lin and C. Lee, J. Electrochem. Soc. **146**, 3466 (1999).
[31]H. Kim, C. Lavoie, M. Copei, W. Narayanan, D. G. Park, and S. M. Rossnagel, J. Appl. Phys. **95**, 5848 (2004).